Research Square

Preprints are preliminary reports that have not undergone peer review.
They should not be considered conclusive, used to inform clinical practice,
or referenced by the media as validated information.

The Role of Adhesion in Triboelectrification Trends: Charge Polarity and Magnitude

Andris Šutka

andris.sutka@rtu.lv

Riga Technical University https://orcid.org/0000-0002-5739-0164

Līva Ģērmane

Linards Lapčinskis

Tianhuai Xu

Jiahao Ye

Jēkabs Grušs

Jin-Chong Tan

University of Oxford https://orcid.org/0000-0002-5770-408X

Article

Keywords:

Posted Date: December 12th, 2025

DOI: https://doi.org/10.21203/rs.3.rs-8249486/v1

License: This work is licensed under a Creative Commons Attribution 4.0 International License.
Read Full License

Additional Declarations: There is **NO** Competing Interest.

Abstract

Triboelectricity – the generation of charge through the contact-separation – underpins technologies including energy harvesting and sensing. While the charge magnitude is known to depend on surface chemistry, morphology, and mechanical properties, the role of adhesion – particularly on charge polarity – remains unclear. Here, we investigate adhesion effects using polydimethylsiloxane (PDMS) films with different base polymer to curing agent ratios (5:1, 10:1, and 15:1), yielding distinct viscoelastic and adhesive properties without altering chemical structure. Nanoindentation and pull-off tests revealed that reduced cross-linking enhances viscoelastic deformation and work of adhesion. Triboelectric measurements demonstrated that more adhesive PDMS surfaces generate more negative charge densities. When PDMS films of differing adhesion were contacted, the more adhesive surface charged negatively, while the less adhesive one positively, enabling polarity control without chemical modifications. Increased contact duration further enhances both adhesion and charge density. These findings reveal that adhesion engineering, offers a simple strategy for optimizing triboelectric charging trends.

Introduction

Triboelectricity is a well-known phenomenon widely observed in daily life. The triboelectric charge manifests as static electricity on the surface of an insulating material. It occurs when materials such as non-conductive polymers are contacted and separated due to mechanical friction and surface adhesion effects. The triboelectric charge has both negative and positive effects. On the one hand, it causes the ignition and damage of electronic devices, but on the other hand, it provides a large variety of applications such as particle separation[1], waste mechanical energy harvesting[2], printing[3], sensing[4], and catalysis[5].

Higher surface charge density forms when materials with differing triboelectric properties undergo contact and separation interaction. Specifically, a material with a positive charging tendency, when paired with a polymer that charges negatively according to the triboelectric series, generates a larger charge output. Recent studies have shown that the magnitude and polarity of triboelectric charge depend on the polymer's mechanical properties, morphology, and adhesion[6–8]. For instance, experiments involving 196 polymer combinations revealed that softer materials tend to acquire a negative charge, while harder materials gain a positive charge[7]. Similarly, when chemically identical polymers are tested, rough surfaces typically charge positively, and smooth surfaces charge negatively[6,9]. Notably, stronger charging occurs when a soft, smooth polymer contacts a hard, rough polymer[6]. Here we will report the effect of adhesion on the polarity of triboelectric surface charge by contacting chemically identical polydimethylsiloxane (PDMS) films with different cross-linking densities.

Several studies have reported the effect of adhesion on triboelectric charging. Ghori et al.[10] discovered that increasing the proportion between hydroxyl and alkyl or silane groups on the cellulose surface led to a significant reduction in both the electrostatic charge and surface adhesion. Additionally, a direct linear

relationship was observed between triboelectric charge and particle surface adhesion. Further, surface adhesion has been suggested as a driving force for heterolytic bond cleavage and mechano-ion (organoion) transfer[11]. The energy associated with this separation is most accurately characterized by the work of adhesion, which defines the energy required to detach two contacted polymer surfaces[12,13].

The adhesion effect can be tuned chemically, by changing the cross-linking degree of the polymer. Maeda et al.[14] found that cross-linked polymers exhibit lower adhesion compared to uncross-linked ones. This reduction is attributed to the restricted mobility of macromolecular chains, which limits their ability to form strong intermolecular bonding at the surface. Adjusting the cross-linking density can thus be an effective strategy for controlling polymer adhesion. Sutka et al. showed that the lower cross-linking density of PDMS increased the separation stress at contact interface from 1.0 N cm^{-2} to 3.4 N cm^{-2} (10–34 kPa) and surface charge density from 0.31 to 3.39 nC cm^{-2} [15].

However, despite extensive research on how adhesion affects triboelectric surface charge density, the effect of surface stickiness on charge polarity remains unexplored. The existing research related to the effect of adhesion on polymer triboelectrification focuses on different material pairings, introducing several variables into the system such as distinct chemical composition[8], hydrophilicity[16] or zeta-potential[17]. Therefore, in this work we explore the impact of adhesion on charge polarity in the same polymer by contacting chemically identical PDMS with different degrees of molecular cross-linking.

Results and Discussion

The surface properties of PDMS samples

To alter the surface adhesion, the samples with different degrees of cross-linking were prepared by changing the ratio between the base polymer and a curing agent (CA), as illustrated in Fig. 1 (A). Three different base polymer and CA ratios were chosen: 5:1, 10:1, and 15:1. Smaller ratio provides sample brittleness while larger ratio results in an incomplete cross-linking[18,19]. The different formulations change the molecular weight between cross-links (Table 1). The determined crosslink densities ρ_K decrease with increasing ratio of base agent to CA.

Dynamic mechanical analysis (DMA) using the nanoindenter probe provided information about the viscoelastic properties of the samples across a range of frequencies (Fig. 1), such as stiffness, energy dissipation, and molecular mobility. Both the storage modulus (E') and loss modulus (E") decreased with reduced cross-linking, reflecting less stiffness and damping capacity in softer composition[20,21]. The most cross-linked composition exhibited the highest moduli, consistent with its lower deformation and higher resistance to detachment observed[22]. For 10:1 and 15:1 compositions, loss tangent values were relatively similar at low frequencies; however, at higher frequencies, the 15:1 composition showed a slight increase in loss tangent. This suggests enhanced energy dissipation in dynamic conditions, likely due its greater molecular mobility and viscoelastic damping, which may further contribute to the

increased work of adhesion observed despite lower pull-off forces (Table 1). The dynamic mechanical analysis provided direct evidence for the changes of mechanical properties resulting from variations in cross-linking. This confirms that deviations from the standard formulation significantly influence the viscoelastic behaviour, stiffness, and energy dissipation capacity.

Further, the surface adhesion of the sample films was examined using both - a macroscopic test and a microscale measurement by nanoindentation. The adhesion values on the macroscopic scale were extracted using the INSTRON testing system by measuring the overall separation force (N) across the entire 2.5 x 2.5 cm^2 sample interface (Table 1). As expected, the higher adhesion was measured for the formulations with the higher ratio between the base polymer and a CA. This is attributed to the enhanced viscoelasticity, lower storage modulus, and greater stress relaxation ability of PDMS with lower cross-linking density. This combination of mechanical properties enable the material to deform more easily, conform more effectively to surface irregularities, and maintain contact during detachment[23–25].

Table 1
Comparison of cross-linking density, molecular weight between cross-links pull-off force, pull-off stress, work of adhesion and separation force of different PDMS compositions.

PDMS composition	Cross-linking density (m^{-3})	Molecular weight between cross-links (g mol^{-1})	Pull-off force (mN)	Pull-off stress (mPa)	Work of adhesion (pJ)	Separation force (N)
5:1	8.76×10^{26}	1416	0.173 ± 0.002	0.082 ± 0.001	196 ± 2	11.15 ± 1.19
10:1	4.64×10^{26}	2676	0.181 ± 0.003	0.085 ± 0.001	273 ± 5	12.30 ± 1.90
15:1	2.85×10^{26}	4350	0.164 ± 0.001	0.077 ± 0.001	304 ± 3	13.75 ± 2.42

The nanoindentation method provides localized measurements at the microscale. By combining macroscale and microscale techniques, it is possible to assess the overall and local adhesion characteristics of the samples. For the 5:1 and 10:1 samples a consistent trend is observed: as the material becomes less cross-linked, all parameters – pull-off force, pull-off stress, and work of adhesion – increase (Table 1). Interestingly, the least cross-linked sample 15:1 deviated from this trend. While it exhibited the highest work of adhesion, both the pull-off force and pull-off stress were lower compared to other compositions. This divergence may be attributed to excessive material deformation, which can reduce effective stress transfer during detachment despite stronger energy dissipation at the interface[25–27]. These results highlight that beyond a certain level of softness, the mechanical response of the material may limit the measurable adhesion forces, even when interfacial bonding is more prominent.

The load-depth curves obtained from nanoindentation (Fig. 2 (A)) further illustrate the distinct adhesion characteristics of the three sample compositions. A representative example of a load–depth (P–h) curve during a pull-off test is shown in Fig. 2 (B), where $\delta_{contact}$ is the indentation depth at the jump-to-contact point, $\delta_{pull-off}$ and $F_{pull-off}$ are the indentation depth and the load at the point of maximum adhesive force, respectively. $W_{adhesion}$ is the work of adhesion incurred during one loading cycle, quantifiable by integrating the shaded area under the $P - h$ curve. For the 5:1 and 10:1 samples, decreasing in cross-linking degree results in curves that are both slightly wider and exhibit higher pull-off force, corresponding to greater resistance during probe detachment and higher work of adhesion. Additionally, the slope of the loading and unloading segments is steeper for the 5:1 composition, reflecting its higher stiffness, which is consistent with the probe DMA results discussed earlier. In contrast, the 15:1 composition displays notably different curve profile – shallower in load (lower $F_{pull-off}$) but significantly broader in depth – indicating that the material undergoes greater viscoelastic deformation and slower recovery during the unloading stage. Despite the lower pull-off force and stress, the increased change of depth during unloading leads to a larger integrated area under the load-depth curve, which translates to a higher calculated work of adhesion (Table 1). This behaviour underscores the role of viscoelastic energy dissipation in soft materials and rubbery polymers (elastomers), where substantial deformation can dominate the adhesion response even when the maximum applied load is reduced[28–30].

Surface chemical properties play a critical role in determining the charge affinity of polymers, which directly impacts their performance in triboelectric generators[31,32]. ATR-FTIR and Raman spectroscopy were employed to detect changes in chemical bonding and molecular structure associated with varying crosslinking levels. These vibrational spectroscopy techniques are suited for identifying functional group modifications and evaluating differences in surface and bulk chemical environments, which may influence charge transfer behaviour and interfacial interactions[33]. Infrared spectroscopy was used to assess the chemical structure of the three PDMS compositions (Fig. 3 (A)). All samples exhibited characteristic peaks associated with PDMS, confirming their consistent base chemistry. Typical absorption bands include Si-CH_3 symmetric and asymmetric deformation modes near 1260 cm^{-1} and 800 cm^{-1} and the Si-O-Si stretching vibration around 1000–1130 cm^{-1} [34]. Notably, subtle but consistent differences were observed between the samples. In the Si-O-Si stretching region (~ 1060 cm^{-1}), which typically presents as a double peak[35], a variation in intensity was evident in the lower part of this feature: the 5:1 composition with the highest cross-linking agent concentration showed the lowest intensity, followed by the 10:1 composition, while the 15:1 composition with the lowest cross-linking agent concentration exhibited the highest intensity of absorbance peak. This trend may reflect differences in siloxane network flexibility or crosslinking density, which influence segmental mobility. The variation in the Si-O-Si stretching intensity is a direct reflection of the cross-linking density and flexibility of the siloxane network. Higher cross-linking agent concentration results in a more rigid network with lower vibrational intensity, while lower concentrations allow for greater flexibility and higher intensity[36,37].

Changes in the intensity of the peak at 910 cm^{-1} are attributed to Si-H asymmetric bending[38]. CA of Sylgard 184 is known to possess both Si-H and Si-CH_3 groups along its backbone[39]. From the results, we see that the highest intensity is for 5:1 composition, where CA content is around 17 wt%, while it decreases both for 10:1 composition (CA ≈ 9 wt%) and 15:1 composition (CA ≈ 6 wt%) for which the peak is almost indistinguishable. The presence of Si–H bonds in the CA promotes cross-linking between siloxane backbones containing vinyl groups (Si-C_2H_3) via the hydrosilylation reaction[40]. Results indicate that for the 5:1 composition, there is a larger fraction of unreacted Si-H bonds than in 10:1 or 15:1 compositions, which is in line with results reported in other studies[40].

Raman spectra also displayed the typical peaks associated with PDMS (Fig. 3 (B)). Key Raman-active modes include strong Si-O-Si symmetric stretching near 490 cm^{-1}, Si-C stretching around 710 cm^{-1} and characteristic band near 1410 cm^{-1} corresponding to CH_3 deformation[41]. A subtle difference was observed at approximately 760 cm^{-1}, a region often attributed to Si-CH_3 rocking or bending vibrations[42]. The 5:1 composition showed the most intense peak at his position, while the 10:1 and 15:1 samples exhibited slightly lower intensities. This trend may reflect differences in chain packing or crosslinking density, where a stiffer network structure in the 5:1 sample enhances Raman activity in this mode[20,43]. These Raman findings align with FTIR observations.

These spectroscopic distinctions, though subtle, provide further evidence of underlying structural differences across the compositions that likely contribute to their differing macroscopic behavior. The CA contains both -H and -CH_3 functional groups on Si-O-Si backbone[39]. The hydride groups participate in hydrosilylation with the –CH = CH_2 groups of the base prepolymer, forming Si–CH_2–CH_2–Si crosslink sites (supplementary information, scheme S1). However, the changes in the ratio between C-C bonds and Si-O bonds are small as evident from differences in the peak intensities (< 4%) and shouldn't create an impact on the chemical structure (i.e. charge affinity) of the surface.

The effect of adhesion on triboelectric charge

The three different compositions of PDMS were tested to study the influence of surface adhesion on triboelectric charge, by contacting them against ITO in Faraday cup mode as showed in Fig. 4 (A). The experimental results are presented in Fig. 4 (B) and (C). PDMS samples exhibiting stronger adhesion to ITO also demonstrate larger charge density. The measured separation force curves are presented in supplementary figure S1. With increase in the average adhesion from 11.15 N to 13.75 N the charge density increases and becomes more negative from − 0.18 nC cm^{-2} to − 0.47 nC cm^{-2}. This can be attributed to charge (organoion) transfer due to covalent bond breakage, as the softness and adhesion increases[8,44]. Prior studies have linked organoions as the charge species in contact electrification[45,46], proven via XPS, AFM[11,47], Raman[48] and IR spectroscopy[49]. Furthermore, a clear correlation between adhesion force and surface charge has been observed[8]. In highly adhesive interfaces, the energy of the formed adhesive (physical) bonds between contacting surfaces may exceed the energy of chemical or

physical bonds within the bulk[50]. The increase of adhesion forces enhances the likelihood of covalent bond scission and organoion transfer, contributing to the observed triboelectric effects[8]. On the other hand, softer materials undergo a larger extent of deformation, thus increasing the specific contacting area and enhancing charge transfer[51]. Interestingly, for all compositions, the first separation cycle exhibited a noticeably lower force peak compared to subsequent cycles. As the number of cycles increased, the separation force increased and reached a steady-state value by approximately the 10th cycle as shown in supplementary figure S2. The relative increase in separation force between the first and the tenth cycle was 14%, 9% and 19% for the 5:1, 10:1 and 15:1 compositions, respectively. This can be attributed to electrostatic attraction from triboelectric charges[52] or due to formation of free polymer chains from bond rupture that may entangle with the molecules on the opposite film, thus providing stronger adhesion[14]. When tested against ITO, all three PDMS compositions exhibited the same negative charge polarity. This coincides with the tendency of PDMS to occupy a negative position in the triboelectric series when paired with hard, smooth conductive oxides such as ITO[53–55]. In this case, the nature of the counter surface appears to dominate the polarity outcome, while the differences in base and CA ratio primarily influence the magnitude of the generated charge.

To reveal the effect of adhesion on charging tendencies, we tested PDMS vs. PDMS samples with the same or different CA ratio (Fig. 5 (A), (B) and (C)). Contacting PDMS films with similar surface adhesion produced a negligible charge of 0.002 nC cm^{-2}. This is attributed to the same extent as bi-directional material transfer. It is known that bidirectional material transfer occurs between contacted polymers[56]. Both positive and negative organoions may be transferred, forming the so-called surface charge mosaics[57]. If the mechanical hardness, morphology, and adhesion are the same for both contacted polymer films, the same amount of charges will be exchanged between the two surfaces, and the net surface charge density will be zero.

When two PDMS films with different adhesion were contacted, the surface charge increased by an order of magnitude. The surface charge 0.06 nC cm^{-2} was measured by contacting PDMS 5:1 vs. PDMS 15:1, which is 6 times higher result than the combination of 5:1 vs. 10:1 and 30 times higher if compared to TENG made out of the same composition PDMS (Fig. 5(D)). These results highlight the critical role of surface adhesion in triboelectric charge generation.

Prior studies have shown that this process is strongly influenced by mechanical softness. It has been reported[11,47] that soft polymers tend to undergo greater mass transfer during contact, with transfer occurring in both directions but predominantly from the softer material to the harder one. Additionally, our group has previously shown[7] that when different polymers are contacted, softer material typically becomes negatively charged while the harder material charges positively. Regarding PDMS polarity, Pandey et al[11] showed that when PDMS films with different stiffnesses (*E*) are contacted against much more rigid PVC, the less crosslinked (lower *E*) PDMS charges more negatively than the more crosslinked formulation (higher *E*). Our results therefore extend existing theory by demonstrating that, even in

chemically identical elastomers, adhesion-mediated differences in mechanical response are sufficient to switch the sign of the charge polarity.

More interestingly, we observe that the stickier surface of two PDMS mutually contacted surfaces charges negatively, while the surface with lower adhesiveness charges positively (Fig. 5 (E)). Coincidently, the more adhesive surface is the one with lower crosslink density and lower *E*, thus providing increased chain mobility and greater conformity to the asperities of the contacted surface. This observation reveals the polarity of the triboelectric charge can be tuned through surface adhesion/crosslink density. This represents a significant advancement in the understanding of triboelectric phenomena, demonstrating that polarity—previously considered a material-specific property—can be modulated through physical modifications of the surface, without substantially altering its chemistry. Since bond scission is expected in the material with least crosslinks (lower *E*), mass transfer most likely occurs from the most adhesive PDMS surface to the least adhesive PDMS. Given that most elastomers tend to charge negatively[58–60], enhancing adhesion offers a practical route to boost charge density and tailor polarity in device design simultaneously, especially in configurations where the same material is used for both triboelectric layers.

Influence of compression time to change the interfacial adhesion

To further investigate the role of contact conditions, we conducted additional measurements in the Instron tester focusing on the effect of contacting time on both charge generation and interfacial adhesion. It is expected that increased contact time will result in stronger separation force and surface charge. PDMS film samples were tested against ITO electrode in the Faraday cup mode as shown before in Fig. 4 (A). The results reveal that both charge density and separation force are strongly dependent on the compression time linked to the stress relaxation of elastomers (Fig. 6 (A)).

Separation force initially increases with compression time, reaching a maximum value at approximately 240 seconds, after which a gradual decline is observed. This behaviour suggests that a more prolonged contact enhances interfacial interactions, possibly due to the formation of more adhesive intermolecular bonds, molecular rearrangement, or improved contact conformity as a function of time[61,62]. The subsequent decrease may be due to viscoelastic relaxation[63,64]. A similar trend is seen in charge density, which also sharply increases and then slightly decreases. Notably, a correlation is observed between separation force and absolute values of charge density (Fig. 6 (B)), indicating that compression time induced adhesiveness follows a trend where higher stickiness between PDMS and ITO results in more negative charge.

Conclusion

In this work, the mechanical properties and surface adhesion of PDMS was effectively varied by changing the degree of crosslinking. The least crosslinked PDMS shown pronounced mechanical softness, as well as highest separation force and work of adhesion. Moreover, the less cross-linked

PDMS also shown tendency to exhibit a larger surface charge density upon contact-separation versus ITO due to enhanced specific contacting area and organoion transfer. Upon identical PDMS vs PDMS material contact the more adhesive (less cross-linked) surface acquired negative surface charge, while the less adhesive PDMS became positively charged. This work demonstrates the significance of surface adhesion on triboelectric charge density and polarity. This new knowledge can be used to tune the triboelectric charging of materials in future.

Methods

Sample preparation

PDMS (DOW, Sylgard™ 184) samples were made by mixing base polymer and CA in different weight ratios (5:1; 10:1, and 15:1) and spin-coated on the indium tin oxide (ITO) substrate at 2500 rpm for 10 s. Then, the PDMS samples were cured at 80°C for 24 h. The size of the obtained sample films was 5 cm^2 and the thickness was 100 μm.

Material characterization

Attenuated total reflectance Fourier transform infrared spectroscopy (ATR-FTIR) spectroscopy measurements were performed to determine structural differences of various compositions of PDMS by using Nicolet iS10 FTIR spectrometer equipped with an attenuated total reflectance (ATR) module.

The chemical composition was studied using Raman spectroscopy which was performed with Renishaw InVia Reflex confocal Raman microscope. Raman spectra were collected in the range of 300 to 1700 cm^{-1} under irradiation with 514 nm laser using 20 mW laser power.

To study the mechanical properties, probe-based dynamic mechanical analysis (probeDMA) was performed implementing the technique developed for the KLA iMicro nanoindenter. A flat-ended diamond cylindrical punch (radius = 26 μm) was used to apply an oscillating stress on the sample at varying frequency, and the resultant displacement oscillation was recorded to reveal information about the storage modulus, loss modulus and the loss tangent of the viscoelastic sample. The storage modulus (E') is a measure of stored energy under deformation and quantifies the elastic property of the sample. The loss modulus (E'') quantifies the viscous response, and it measures energy dissipation during loading cycle. The ratio of loss modulus and storage modulus gives the loss tangent ($\tan\delta = E''/E'$), which characterizes damping in the material by energy dissipation. A total of 16 tests were performed in 4 discrete regions on a 2.5 × 2.5 cm^2 nominal sample area, and 4 points were selected in each region. Using the obtained storage moduli values at 1 Hz, the molecular weight between crosslinks (M_C) was calculated with the formula

$$M_C = 3\rho\, R_{\mathrm{g}} T E^{-1}$$

1

where ρ is the density of polymer, R_g the gas constant and T the absolute temperature[65]. Crosslink densities were calculated using formula

$$E = \frac{3}{2} kT\rho_K$$

2

where E is tensile modulus, k is the Boltzmann constant, and T is the absolute temperature[66]. As the loss tangent at 1 Hz frequency is low (under 0.08), indicating that the material response was elastic, we can assume that storage modulus E' is a good approximation of tensile Young's modulus E for the purpose of calculating crosslink density[67].

During the pull-off test performed in the iMicro nanoindenter, a cylindrical flat punch with a radius of 26 μm was initially withdrawn 2 μm from the sample surface, ensuring that the tip was fully out of the adhesion interaction zone. The tip then started approaching the surface at a speed of 100 nm s^{-1} until it was in the vicinity of the surface. To allow more accurate surface detection, the phase signal was monitored in this process until a phase change larger than 15° was detected. After contacting the surface, an indent was performed at a loading rate of 0.01 mN s^{-1} to a maximum load of 0.1 mN. The tip was held in peak load position for 2 s before it was unloaded at the same rate, and eventually withdrawn 5 μm from the sample surface. The nominal pull-off stress was determined by dividing the pull-off force by the contact area of the flat-ended punch (nominal area = 2124 μm^2). Pull-off force and pull-off stress values were averaged from 12 measurements performed on different regions of the same sample. The work of adhesion was determined by calculating the enclosed area established under the load-depth curve. A total of 12 tests were performed in 3 discrete regions on a 2.5 × 2.5 cm^2 sample area and 4 points were selected in each region. Work of adhesion values were calculated by integrating the area under the load-depth curve and averaged from 12 separate measurements.

Triboelectric measurements

The contact-separation study was carried out using an Instron E1000 material testing machine, which ensures the repeatability of triboelectric measurements. They were performed under controlled conditions – a separation distance of 5 mm, a compression force of 10 N, and a separation speed of 0.1 m s^{-1}. The generated current signals were measured using a Keithley 6514 electrometer connected to a Picoscope 5444B PC oscilloscope system. Surface charges, Q (nC), were calculated by

$$Q = \int i\, dt$$

3

where *i* is the instantaneous current (nA) and d*t* is the differential of time (s). Integration was done for the high, narrow peaks, which correspond to the separation stage. The charge generated by individual PDMS films was determined after contact-separation with ITO, which was connected to an electrometer, and the current was measured against ground. This measurement setup was used as a Faraday cup mode to determine the magnitude and polarity of triboelectric charges formed on the PDMS samples, as well as to measure the force (N) necessary for separation of PDMS films. Three parallel sets of sample pairs were tested for each combination. The separation force values were taken from dynamic mechanical tests and averaged from 20 separation peaks of each sample. The separation force difference (*ΔN*) between two PDMS samples was calculated as

$$\Delta N = N_1 - N_2$$

4

where N_1 and N_2 represent separation forces obtained from separate tests of each composition against ITO. This allowed us to isolate the intrinsic triboelectric properties of each PDMS composition sample before testing them against one another, reducing the effect of adhesion and mass transfer between PDMS surfaces. The PDMS films were also used to prepare triboelectric generator. For triboelectric generator tests, the electrometer was connected to both electrodes, therefore measuring the current induced in the outer circuit by potential difference on both contact layers.

Data availability

The data supporting the findings of this study are available in the main text and Supplementary Information, or available from the corresponding author upon reasonable request.

Declarations

Competing interests

The authors declare no competing interests.

Funding

declaration

Līva Ģērmane acknowledges the support by the EU Recovery and Resilience Facility within Project No. 5.2.1.1.i.0/2/24/I/CFLA/003 “Implementation of consolidation and management changes at Riga Technical University, Liepaja University, Rezekne Academy of Technology, Latvian Maritime Academy and Liepaja Maritime College for the progress towards excellence in higher education, science and innovation” academic career doctoral grant (ID 1031).

Author contributions

Līva Ģērmane: methodology, investigation, formal analysis, data curation, visualization, funding acquisition. Linards Lapčinskis: formal analysis, supervision, conceptualization. Tianhuai Xu, Jiahao Ye and Jēkabs Grušs: investigation. Jin-Chong Tan and Andris Šutka: conceptualization and supervision. Writing – original draft was equally contributed by all the authors.

Acknowledgements

The authors thank Anna Šutka for her assistance with visual formatting.

References

1. Shen, Y. *et al*. An experimental study of triboelectrostatic particle charging behavior and its associated fundamentals. *Powder Technol*. 429, 118880 (2023).
2. Bhaduri, A. & Ha, T.-J. Biowaste-derived triboelectric nanogenerators for emerging bioelectronics. *Adv. Sci.* 11, 2405666 (2024).
3. Kopp, S.-P. *et al*. Enabling triboelectric charging as a powder charging method for electrophotographic powder application in laser-based powder bed fusion of polymers by triboelectric charge control. *Addit. Manuf.* 68, 103531 (2023).
4. Pal, A. *et al*. Construction of triboelectric series and chirality detection of amino acids using triboelectric nanogenerator. *Adv. Sci.* 11, 2307266 (2024).
5. Zhao, J. *et al*. Enhanced electrocatalytic synthesis and degradation enabled by triboelectric effect. *Nano Energy* 139, 110962 (2025).
6. Verners, O. *et al*. Smooth polymers charge negatively: controlling contact electrification polarity in polymers. *Nano Energy* 104, 107914 (2022).
7. Sherell, P. C. *et al*. Probing contact electrification: a cohesive sticky problem. *ACS Appl. Mater. Interfaces.* 13, 44935–44947 (2021).
8. Lapčinskis, L. *et al*. The adhesion-enhanced contact electrification and efficiency of triboelectric nanogenerators. *Macromol. Mater. Eng.* 305, 1900638 (2020).
9. Ģērmane, L. *et al*. Physical and chemical surface modification of recycled polystyrene films for improved triboelectric properties. *Energy Technol*. 12, 2400762 (2024).
10. Ghori, M. U., Šupuk, E. & Conway, B. R. Tribo-electrification and powder adhesion studies in the development of polymeric hydrophilic drug matrices. *Materials* 8, 1482–1498 (2015).
11. Pandey, R. K., Kakehashi, H., Nakanishi, H. & Soh, S. Correlating material transfer and charge transfer in contact electrification. *J. Phys. Chem. C.* 122, 16154–16160 (2018).
12. Šutka, A. *et al*. Engineering polymer interfaces: a review toward controlling triboelectric surface charge. *Adv. Mater. Interfaces*. 10, 2300323 (2023).

13. Jabbari, E. & Peppas, N. A. Polymer-polymer interdiffusion and adhesion. *J. Macromol. Sci., Polym. Rev.* 34, 205–241 (1994).
14. Maeda, N., Chen, N., Tirrell, M. & Israelachvili J. N. Adhesion and friction mechanisms of polymer-on-polymer surfaces. *Science* 297, 379–382 (2002).
15. Šutka, A. *et al*. The role of intermolecular forces in contact electrification on polymer surfaces and triboelectric nanogenerators. *Energy Environ. Sci.* 12, 2417–2421 (2019).
16. Jimidar, I. S. M. *et al*. Influence of wettability and geometry on contact electrification between nonionic insulators. *ACS Appl. Mater. Interfaces.* 15, 42004–42014 (2023).
17. McCarty, L. S. & Whitesides, G. M. Electrostatic charging due to separation of ions at interfaces: Contact electrification of ionic electrets. *Angew. Chem., Int. Ed.* 47, 2188–2207 (2008).
18. Varner, H. & Cohen, T. Explaining the spread in measurement of PDMS elastic properties: influence of test method and curing protocol. *Soft Matter* 20, 9174–9183 (2024).
19. Sales, F. C.P., Ariati, R. M., Noronha, V. T. & Ribeiro, J. E. Mechanical characterization of PDMS with different mixing ratios. *Procedia Structural Integrity* 37, 383–388 (2022).
20. Babu, A. R. & Gundiah, N. Contributions of network topological structures to the mechanical properties of PDMS elastomers. *Mater. Res. Express.* 5, 085310 (2018).
21. Niamlang, S. & Sirivat, A. Electromechanical responses of a crosslinked polydimethylsiloxane. *Macromol. Symp*. 264, 176–183 (2008).
22. Chano, K., Poliskie, G. M. & Fregoso, J. Rheology of thermal interface materials composed of silicone gels. *IEEE Trans. Compon., Packag., Manuf. Technol*. 7, 217–220 (2017).
23. Valentin, J. D. P. *et al*. Substrate viscosity plays an important role in bacterial adhesion under fluid flow. *J. Colloid Interface Sci*. 552, 247–257 (2019).
24. Cai, C. *et al*. Enhanced electromechanical properties of three-phased polydimethylsiloxane nanocomposites via surface encapsulation of barium titanate and multiwalled carbon nanotube with polydopamine. *Macromol. Mater. Eng.* 306, 2100046 (2021).
25. Sakasegawa, D. *et al*. Effects of degree of cross-links on adhesion curves of cross-linked polymers observed by a point-contact method. *Langmuir* 26, 5856–5863 (2010).
26. Bistac, S., Galliano, A. & Schmitt, M. Nanofriction of polymers: the complex role of adhesion. *J. Phys.: Condensed Matter*. 20, 354015 (2008).
27. Dorogin, L. & Persson, B. N. J. Contact mechanics for polydimethylsiloxane: from liquid to solid. *Soft Matter*. 14, 1142–1148 (2018).
28. Li, Z., Yu, H. & Wang, J. Contact creep behavior of polydimethylsiloxane and influence of load, tip size, and crosslink density. *Tribol. Lett.* 49, 291–299 (2013).
29. Cai, J.-H., Huang, M.-L., Chen, X.-D. & Wang, M. Controllable construction of cross-linking network for regulating on the mechanical properties of polydimethylsiloxane and polydimethylsiloxane/carbon nanotubes composites. *J. Appl. Polym. Sci.* 139, 52113 (2022).

30. Qian, S. *et al*. The viscoelastic response of soft material: A theoretical and experimental study based on barreling deformation. *Polym. Test.* 70, 474–480 (2018).
31. Bunk, J. K. G. *et al*. Studying the influence of chemical structure on the surface properties of polymer films. *Colloids Surf., A*. 362, 47–57 (2010).
32. Németh, E., Albrecht, V., Schubert, G. & Simon, F. Polymer tribo-electric charging: dependence on thermodynamic surface properties and relative humidity. *J. Electrost*. 58, 3–16 (2003).
33. Li, S. *et al*. Contributions of different functional groups to contact electrification of polymers. *Adv. Mater.* 32, 2001307 (2020).
34. Johnson, L. M. *et al*. Elastomeric microparticles for acoustic mediated bioseparations. *J. Nanobiotechnol*. 11, 22 (2013).
35. Nakamura, K. & Ichimura, S. Vibrational spectroscopic study of the interface of SiO_2/Si(100) fabricated by highly concentrated ozone: Direct evidence for less strained Si–O–Si bond angle. *Jpn. J. Appl. Phys.* 44, 7602 (2005).
36. Alexandru, M. Siloxane-organic networks in *Recent developments in silicone-based materials* (ed. Cazacu, M.) 107–133 (Nova Science Publishers, Inc., 2010).
37. Li, R. *et al*. Robustly curing epoxy novolacs by linear and cyclic siloxane-functionalized eugenol: Impact of topologies of cross-linkers on properties of thermosets. *ACS Appl. Mater*. 6, 756–767 (2024).
38. Wójcik-Bania, M. Influence of the addition of organo-montmorillonite nanofiller on cross-linking of polysiloxanes – FTIR studies. *Spectrochim. Acta, Part A*. 252, 119491 (2021).
39. Lisensky, G. C. *et al*. Replication and compression of surface structures with polydimethylsiloxane elastomer. *J. Chem. Educ.* 76, 537 (1999).
40. Cho, H. S., Moon, H.-Y., Lee, H. S., Kim, Y. T. & Jeoung, S. C. Formulation prediction for Young's modulus of poly(dimethylsiloxane) by spectroscopic methods. *Bull. Korean Chem. Soc.* 42, 1225–1231 (2021).
41. Borjanović, V. *et al*. Influence of proton irradiation on the structure and stability of poly(dimethylsiloxane) and poly(dimethylsiloxane)-nanodiamond composite. *J. Vac. Sci. Technol. B.* 27, 2396–2403 (2009).
42. Roychowdhury, T., Cushman, C. V., Synowicki, R. A. & Linford, M. R. Polydimethylsiloxane: Optical properties from 1991 to 1688 nm (0.735–6.49 eV) of the liquid material by spectroscopic ellipsometry. *Surf. Sci. Spectra.* 25, 026001 (2018).
43. Bae, S. C., Lee, H., Lin, Z. & Granick, S. Chemical imaging in a surface forces apparatus: Confocal Raman spectroscopy of confined poly(dimethylsiloxane). *Langmuir* 21, 5685–5688 (2005).
44. Fu, H. *et al*. Understanding contact electrification via direct covalent bond cleavage of polymer chains for ultrahigh electrostatic charge density. *Energy Environ. Sci.* 17, 3776–3787 (2024).
45. Baytekin, B., Baytekin H. T. & Gryzbowski, B. A. What really drives chemical reactions on contact charged surfaces? *J. Am. Chem. Soc.* 134, 7223–7226 (2012).

46. Sakaguchi, M., Makino, M., Ohura, T. & Iwata, T. Contact electrification of polymers due to electron transfer among mechano anions, mechano cations and mechano radicals. *J. Electrost*. 7, 412–416 (2014).
47. Baytekin, H. T., Baytekin, B., Incorvati, J. T. & Gryzbowski, B. A. Material transfer and polarity reversal in contact charging. *Angew. Chem., Int. Ed.* 51, 4843–4847 (2012).
48. Puhan, D. & Wong, J. S. S. Properties of polyetheretherketone (PEEK) transferred materials in a PEEK-steel contact. *Tribol. Int*. 135, 189–199 (2019).
49. Yang, P. *et al*. Radical anion transfer during contact electrification and its compensation for charge loss in triboelectric nanogenerator. *Matter* 6, 1295–1311 (2023).
50. Ghatak, A., Vorvolakos, K., She, H., Malotky, D. L. & Chaudhury, M. K. Interfacial rate processes in adhesion and friction. *J. Phys. Chem. B.* 104, 4018–4030 (2000).
51. Kleyman, G., Kang, T., Twiefel, Jens & Voit, W. Characterization of triboelectric charge generation between PTFE and nylon after repeated contacts. *Energy Harvesting and Systems* 4, 165–176 (2017).
52. Wu, J., Zhu, W., Wen, Q., Cao, J. & Cao, Q. Effect of contact electrification on the adhesion behavior of copper/polydimethylsiloxane interface: an atomic-scale investigation. *Appl. Surf. Sci.* 704, 163397 (2025).
53. Ģērmane, L., Lapčinskis, L., Iesalnieks, M. & Šutka, A. Surface engineering of PDMS for improved triboelectrification. *Mater. Adv.* 4, 875–880 (2023).
54. Ye, J. *et al*. Functionalized PDMS for regulating the triboelectric output of nanogenerators: a study of charge transfer mechanisms. *J. Mater. Chem. C.* 13, 7654–7663 (2025).
55. Zhang, R. *et al*. All-inorganic triboelectric nanogenerators based on $Mo_6S_3I_6$ and indium tin oxide. *Nano Energy* 89, 106363 (2021).
56. Lowell, J. Bidirectional charge transfer in repeated contacts to polymers. J. *Electrost.* 20, 233–238 (1987).
57. Baytekin, H. T. *et al*. The mosaic of surface charge in contact electrification. *Science* 333, 308–312 (2011).
58. Burgo, T. A. L., Batista, B. C. & Galembeck, F. Electricity on rubber surfaces: a new energy conversion effect. *ACS Omega* 2, 8940–8947 (2017).
59. Wattanasarn, H., Ngennam, T., Sumpao, T., Thanachayanont, C. & Seetwawan, T. The charging performance in contact electrification of fluorinated ethylene propylene surfaces by electrode bridge. *Sens. Actuators, A.* 346, 113881 (2022).
60. Liu, Y. et al. Enhancement of triboelectric charge density by chemical functionalization. *Adv. Funct. Mater*. 30, 2004714 (2020).
61. Bal-Ozturk, A. *et al*. Tissue adhesives: from research to clinical translation. *Nano Today* 36, 101049 (2021).

62. Lee, J. H. & Lee, D. W. Contact-induced molecular rearrangement of acrylic acid-incorporated pressure sensitive adhesives. *Appl. Surf. Sci.* 500, 144246 (2020).
63. Li, M. *et al*. Effects of bulk viscoelasticity and surface wetting on the contact and adhesive properties of a soft material. *Polym. Test*. 74, 266–273 (2019).
64. Martina, D., Creton, C., Damman, P., Jeusette, M. & Lindner, A. Adhesion of soft viscoelastic adhesives on periodic rough surfaces. *Soft Matter* 8, 5350–5357 (2012).
65. Lamberti, A., Donato, M. D., Chiappone, A., Giorgis, F. & Canavese, G. Tunable electromechanical actuation in silicone dielectric film. *Smart Mater. Struct.* 23, 105001 (2014).
66. Moučka, R., Sedlačík, M., Osička, J. & Pata, V. Mechanical properties of bulk Sylgard 184 and its extension with silicone oil. *Sci. Rep*. 11, 19090 (2021).
67. Kong, D., Meng, Y. & McKenna, G. B. Determination of the molecular weight between cross-links for different ambers: viscoelastic measurements of the rubbery plateau. *Polym. Eng. Sci.* 62, 1023–1040 (2022).

Figures

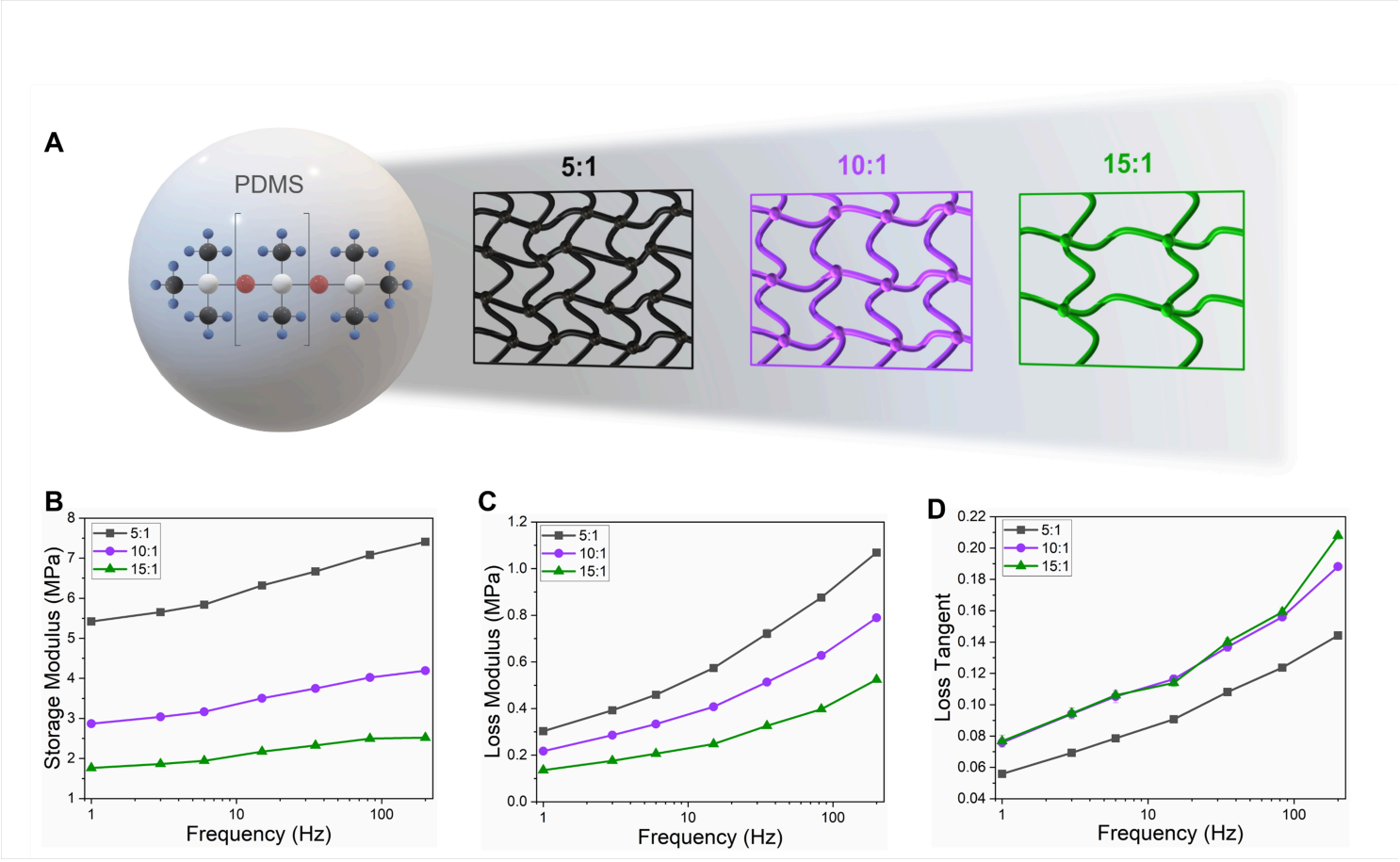


Figure 1

PDMS composition and viscoelastic response under dynamic mechanical loading. (A) Schematic of PDMS molecular structure and 3 different compositions. Comparison of (B) storage modulus (E'), (C) loss modulus (E''), and (D) loss tangent (tan δ) of various PDMS composition samples tested under the probe DMA mode under a flat-punch nanoindenter at frequencies between 1 and 200 Hz.

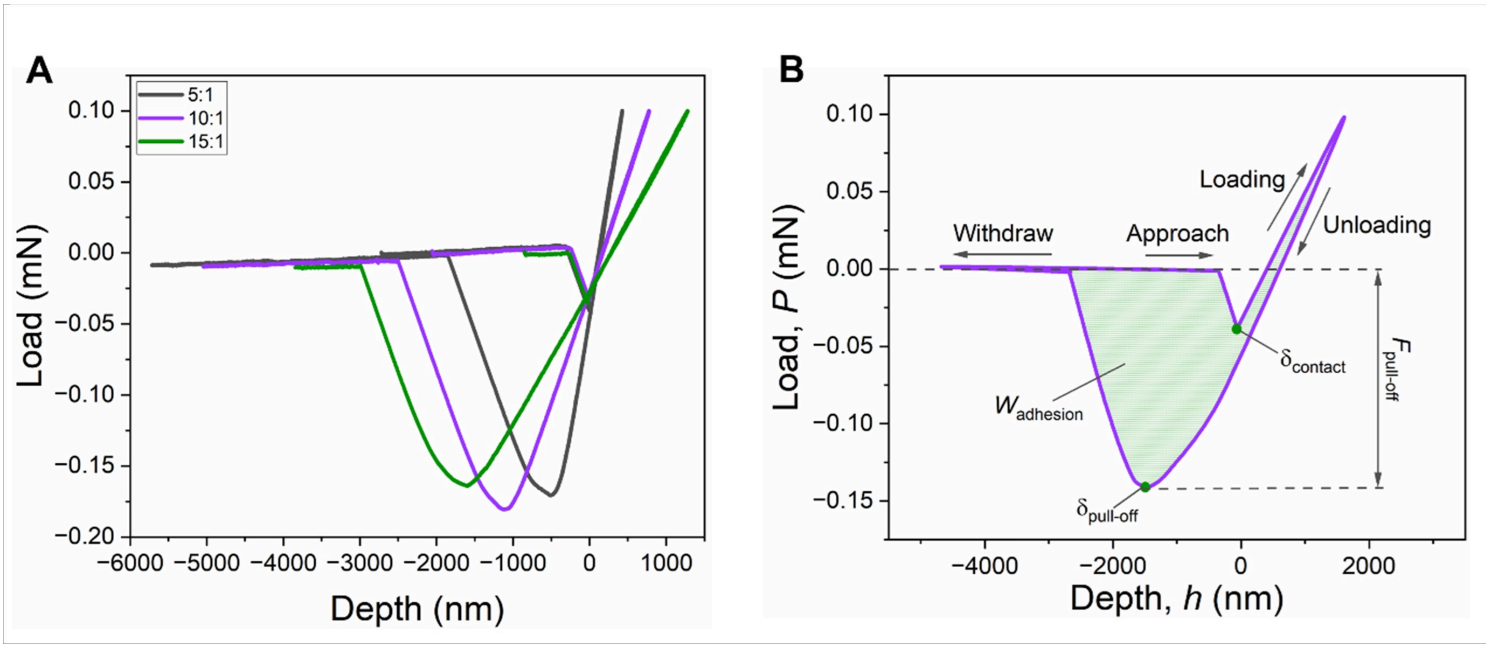


Figure 2

Nanoindentation pull-off response of PDMS. A) Load-depth curves of 3 PDMS compositions during a pull-off test performed by nanoindentation. (B) Schematic illustration of a typical nanoindentation load–displacement curve.

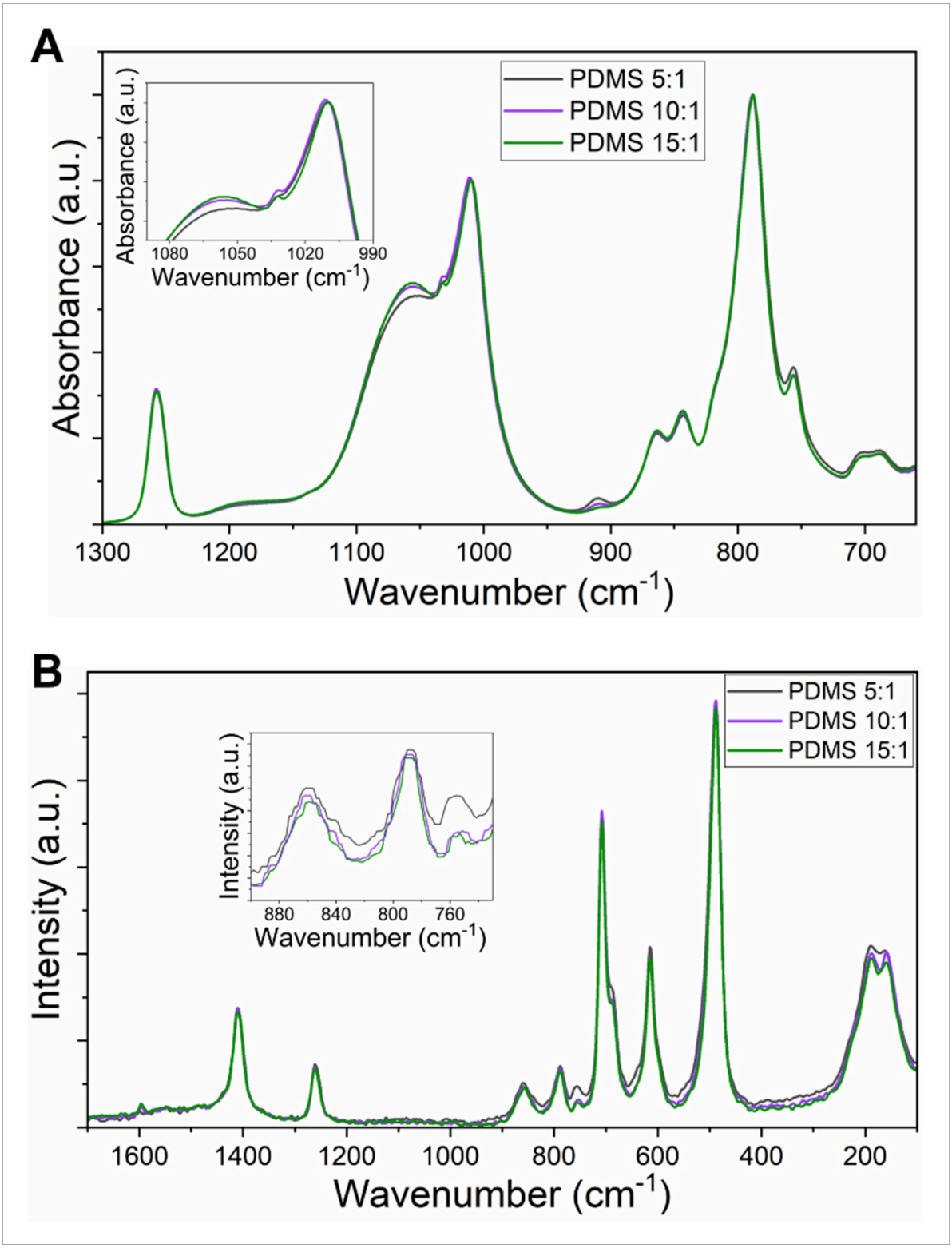


Figure 3

Spectroscopic characterization of PDMS. FTIR (A) and Raman (B) spectra of different PDMS compositions.

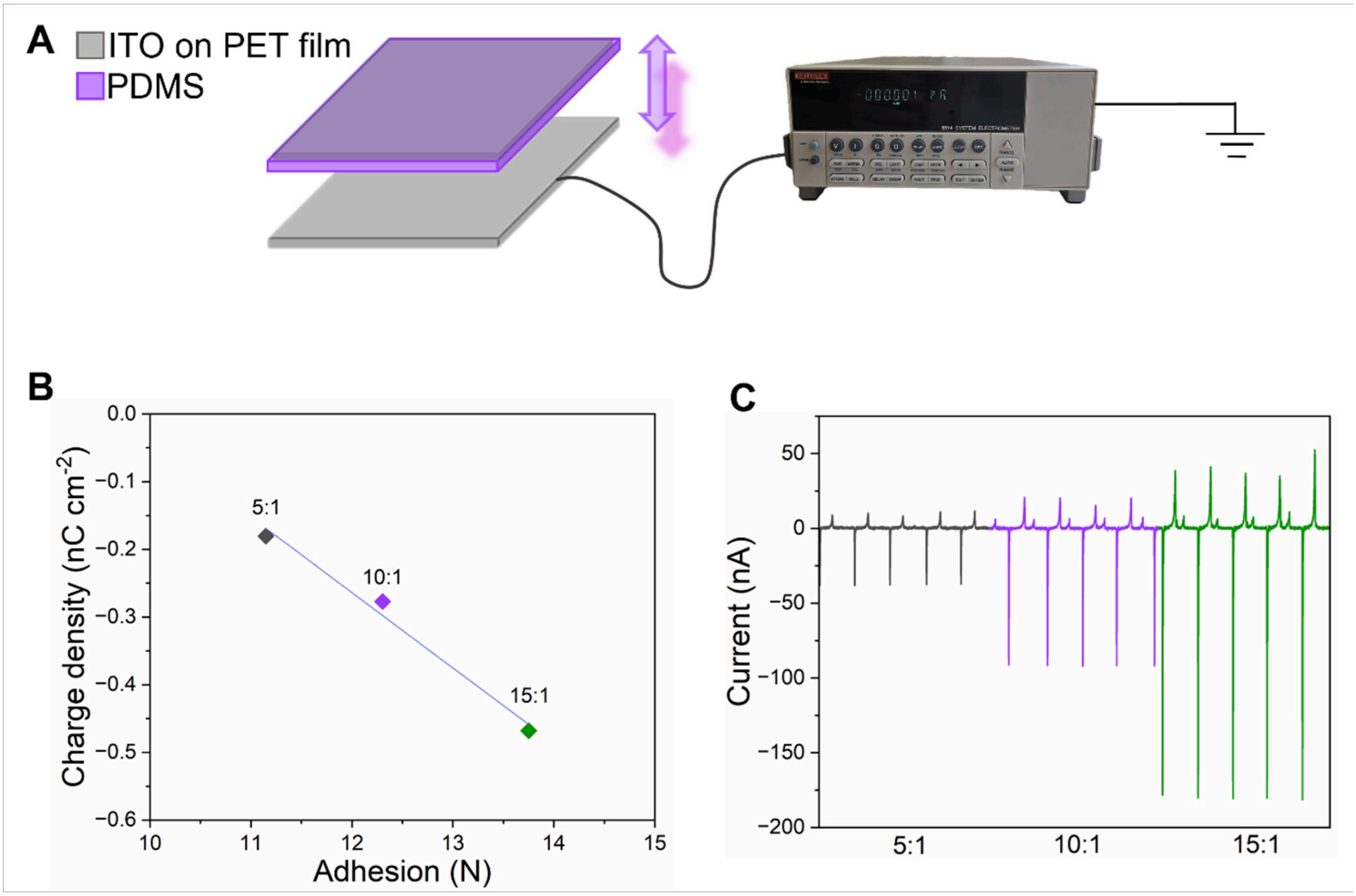


Figure 4

Adhesion-dependent triboelectric response of PDMS. (A) Schematic of Faraday cup setup. Adhesion and charge density correlation (B) and current peaks (C) of various PDMS compositions, tested against ITO in Faraday cup mode.

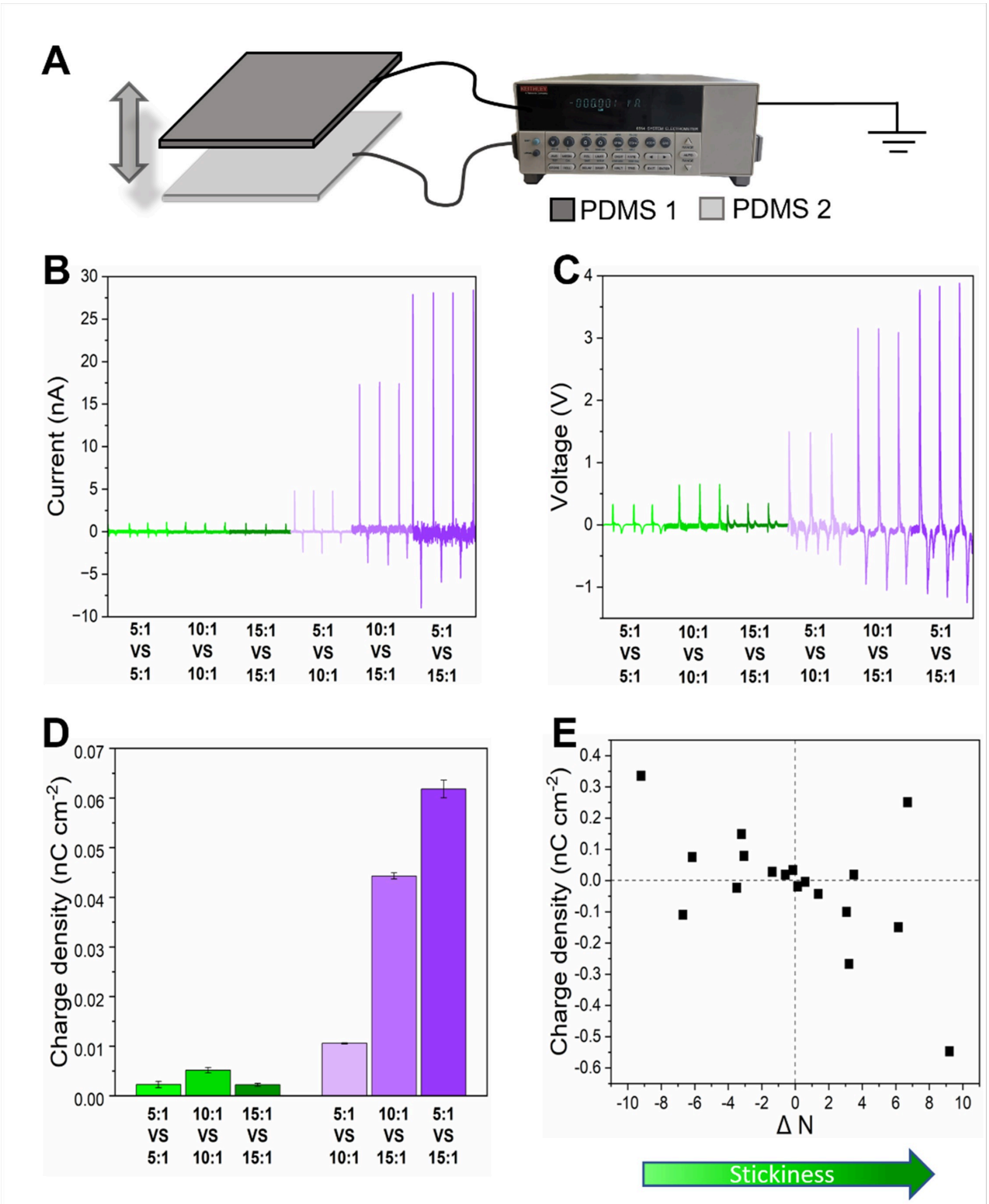


Figure 5

TENG performance and adhesion-dependent charging in PDMS. (A) Schematic of triboelectric generator measurement setup. Current (B) and voltage (C) peaks, charge density (D) of TENG devices made from various PDMS. (E) Dependence of charge density on the adhesion difference between different PDMS.

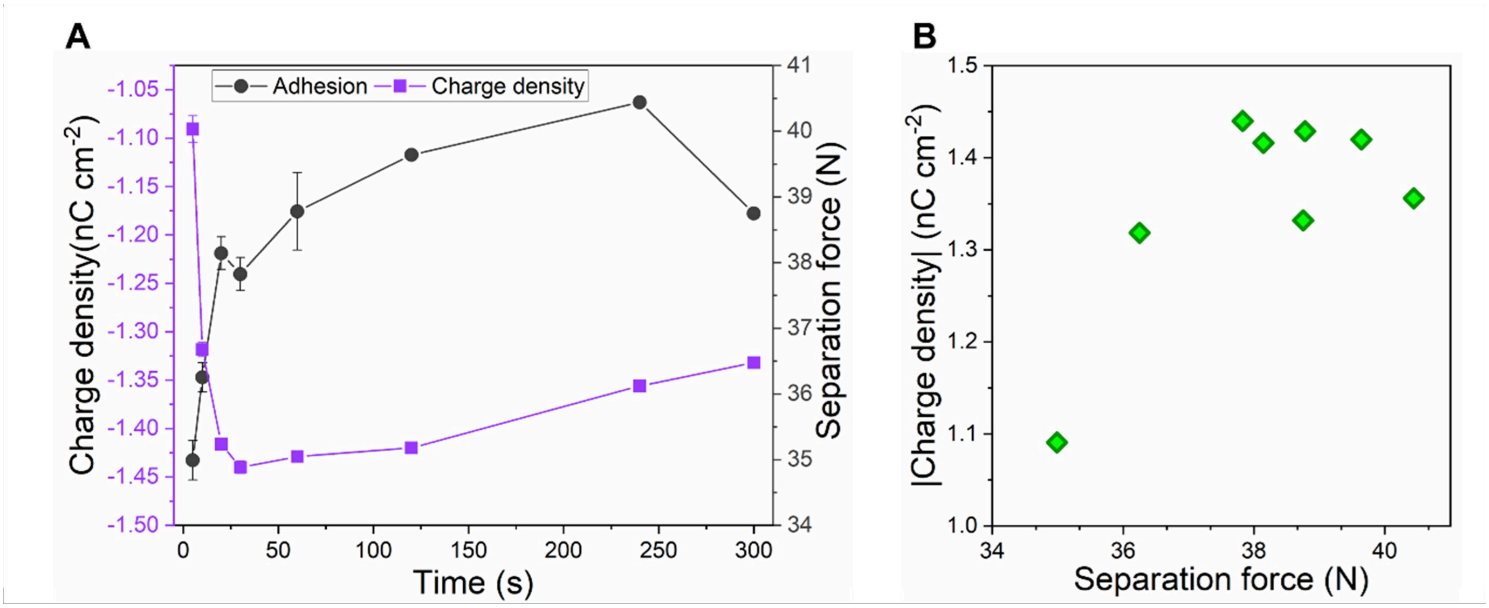


Figure 6

Charge-force relationships in PDMS triboelectric testing. Charge density and separation force dependence on compression time (A) for PDMS, tested against ITO in Faraday cup mode. Charge density dependence on separation force (B) for PDMS.

Supplementary Files

This is a list of supplementary files associated with this preprint. Click to download.

- PDMSadhesionSupplementaryInformation.docx